Autism-associated mutations in K_V7 channels induce gating pore current

Tamer M. Gamal El-Din[a,1,2], Timothy Lantin[a,1], Christopher W. Tschumi[b,1], Barbara Juarez[b], Meagan Quinlan[b], Julia H. Hayano[b], Jin Li[a], Larry S. Zweifel[a,b,2], and William A. Catterall[a,2]

[a]Department of Pharmacology, University of Washington, Seattle, WA 98195; and [b]Department of Psychiatry & Behavioral Sciences, University of Washington, Seattle, WA 98195

Contributed by William A. Catterall, September 16, 2021 (sent for review July 9, 2021; reviewed by Peter C. Ruben and Mark S. Shapiro)

Autism spectrum disorder (ASD) adversely impacts >1% of children in the United States, causing social interaction deficits, repetitive behaviors, and communication disorders. Genetic analysis of ASD has advanced dramatically through genome sequencing, which has identified >500 genes with mutations in ASD. Mutations that alter arginine gating charges in the voltage sensor of the voltage-gated potassium (K_V) channel K_V7 (KCNQ) are among those frequently associated with ASD. We hypothesized that these gating charge mutations would induce gating pore current (also termed ω-current) by causing an ionic leak through the mutant voltage sensor. Unexpectedly, we found that wild-type K_V7 conducts outward gating pore current through its native voltage sensor at positive membrane potentials, owing to a glutamine in the third gating charge position. In bacterial and human K_V7 channels, gating charge mutations at the R1 and R2 positions cause inward gating pore current through the resting voltage sensor at negative membrane potentials, whereas mutation at R4 causes outward gating pore current through the activated voltage sensor at positive potentials. Remarkably, expression of the $K_V7.3$/R2C ASD-associated mutation in vivo in midbrain dopamine neurons of mice disrupts action potential generation and repetitive firing. Overall, our results reveal native and mutant gating pore current in K_V7 channels and implicate altered control of action potential generation by gating pore current through mutant K_V7 channels as a potential pathogenic mechanism in autism.

potassium channels | voltage sensor | autism | gating pore current | gating charges

Autism spectrum disorder (ASD) is a neurological developmental disability that generally appears in children before the age of 3 y (1). ASD results in a wide spectrum of symptoms, including deficits in social interaction, cognitive function, and communication skills and repetitive behaviors. ASD is caused by a complex interaction of environmental and genetic factors. Recently, our understanding of the genetic causes of ASD has increased significantly. There is a high genetic heritability in autism, and complete genome sequencing of an affected individual plus an unaffected sibling and two unaffected parents (trios) has identified more than 500 genes with mutations that are now linked to ASD (2, 3). Cluster analysis of these genes revealed an unexpected number of voltage-gated ion channels (4), and further sequence comparisons revealed overrepresentation of mutations in the Arg residues that serve as the gating charges of their voltage sensors (SI Appendix, Fig. S1) (4). Such mutations are expected to alter the voltage-dependent control of opening and closing of ion channels.

The voltage-gated potassium (K_V) channel K_V7 (KCNQ) ranked high among the ion channel genes having mutations in individuals with neurodevelopmental disorders (4). The K_V7 channels in brain are formed from heterotetramers of $K_V7.2$ and $K_V7.3$, $K_V7.3$ and $K_V7.4$, or $K_V7.3$ and $K_V7.5$ (5), with $K_V7.2/7.3$ being the most prevalent (Fig. 1*A*) (6, 7). K_V7 heteromultimers conduct a tonic inhibitory current that is modulated by Gq-coupled receptors, most notably muscarinic acetylcholine receptors, for which K_V7 current is often termed M current (5, 6, 8). K_V7 heteromultimers are expressed in both excitatory and inhibitory neurons, particularly at axon initial segments and at nodes of Ranvier (9), where they help to set the resting membrane potential and regulate the firing threshold and frequency. Conditional deletion of $K_V7.2$ from cerebral cortex causes hyperexcitability (10). Deletion of $K_V7.2/7.3$ channels also causes hyperexcitability of inhibitory parvalbumin-expressing interneurons, but this ultimately leads to homeostatic potentiation of excitatory transmission between pyramidal neurons (11). Genetic or pharmacological reduction of the K_V7 current causes epilepsy (e.g., benign familial neonatal convulsions) (12, 13). As these examples demonstrate, K_V7 channels are broadly important in control of action potential firing and in loss of control of electrical excitability in neurological disease, and as such, pharmacological interventions at K_V7 channels may have value in multiple neurological and psychiatric diseases (14).

Like other K_V channels, K_V7 is composed of four subunits having six transmembrane segments (S1 to S6) (15). The S1 to S4 segments form the voltage sensor, whereas the S5 and S6 segments form the pore (15). The S4 segments of K_V channels generally contain four or more repeated motifs of a positively charged residue, usually arginine (Arg), flanked by two

Significance

Autism spectrum disorder (ASD) adversely impacts >1% of children, causing social interaction deficits, repetitive behaviors, and communication disorders. Genetic analysis of ASD has advanced dramatically through genome sequencing, which has identified >500 genes with mutations in ASD. Mutations in the voltage sensor of the voltage-gated potassium (K_V) channel K_V7 are frequently associated with ASD. We discovered that these ASD mutations cause an ionic leak through the voltage sensor, termed gating pore current. When these mutations were inserted into the genome of mouse dopamine neurons, they caused a dramatic alteration in the ability of those neurons to fire action potentials in response to electrical stimulation. These changes would impair information processing in neurons, leading to broad changes in brain function.

Author contributions: T.M.G.E.-D., T.L., C.W.T., L.S.Z., and W.A.C. designed research; T.M.G.E.-D., T.L., C.W.T., B.J., M.Q., J.H.H., and J.L. performed research; T.M.G.E.-D., T.L., C.W.T., B.J., M.Q., and L.S.Z. analyzed data; and T.M.G.E.-D., C.W.T., B.J., L.S.Z., and W.A.C. wrote the paper.

Reviewers: P.C.R., Simon Fraser University; and M.S.S., University of Texas Health San Antonio.

The authors declare no competing interest.

[1]T.M.G.E.-D., T.L., and C.W.T. contributed equally to this work.

[2]To whom correspondence may be addressed. Email: tmgamal@uw.edu, larryz@uw.edu, or wcatt@uw.edu.

This article contains supporting information online at http://www.pnas.org/lookup/suppl/doi:10.1073/pnas.2112666118/-/DCSupplemental.

Published November 2, 2021.

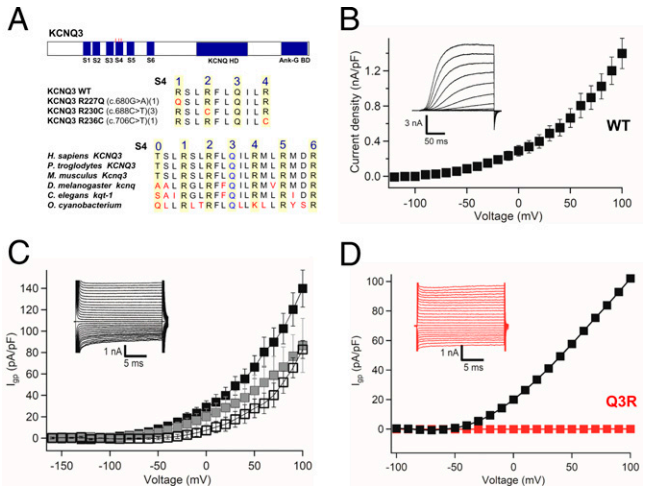

Fig. 1. Gating pore currents in bacterial potassium channel K_V7Oc. (*A*) Bioinformatic analysis of ASD mutations in ion channels. (*B*) Central pore K^+ currents (*Inset*) and conductance–voltage (G–V) curve for K_V7Oc during 200-ms depolarizations from −100 mV to the indicated potentials. (*C*) Wild-type gating pore Cs^+ currents (I_{gp}) (*Inset*) from different holding potentials: −100 mV (black squares), −50 mV (gray squares), and 0 mV (open squares). n = 5 to 10. (*D*) Blocking of wild-type Cs^+gating pore current by Q3R mutation. P = 0.001; Student's t test, two sided.

hydrophobic residues (15). These positively charged residues serve as gating charges that respond to depolarization and repolarization by moving outward and inward across the hydrophobic constriction site, which seals the voltage sensor (15–17). Voltage-dependent movements of the S4 segment driven by the gating charges are conformationally coupled to opening and closing the pore (15–17).

The gating charges of voltage-gated sodium and calcium channels in skeletal muscle are targets of mutations that cause hypokalemic periodic paralysis (18). Remarkably, mutation of the gating charge Arg residues causes an ionic leak through the voltage sensor, termed ω-current or gating pore current (19–23). Continuous inward leak of Na^+ through the mutant voltage sensor reduces the sodium gradient in skeletal muscle fibers, depolarizes and creates instability of the membrane potential, and depresses firing of action potentials, leading to flaccid paralysis (21–23). This suggests that gating charge mutations in K_V7 channels could cause gating pore current that is pathogenic in ASD.

We unexpectedly detected robust outward gating pore current in wild-type (WT) K_V7 channels, which depends on a highly conserved Gln (Q) at the third gating charge position that is a conserved Arg (R) in other voltage-gated channels (15). Introducing the ASD-associated gating charge mutations R1Q and R2C at the first and second gating charge positions in K_V7.3 generated inward gating pore current through the mutant voltage sensor, and the ASD-associated gating charge mutation R4C at the fourth gating charge position generated increased outward gating pore current. Dopamine neurons of the ventral tegmental area (VTA) are potently modulated by M current generated by K_V7 channels, which strongly regulates action potential firing and input–output relationships (24–26). These cells play a key role in the regulation of neural networks that control social behavior (27–29), and disrupted function of dopamine neurons is increasingly linked to ASD etiology (30–33). We found that replacing mouse wild-type K_V7.3 with human K_V7.3 containing the ASD mutation R2C markedly disrupted action potential firing in dopamine neurons in brain slices. Collectively, our results support the hypothesis that gating pore current through mutant voltage sensors of K_V7 channels disrupts neural activity and implicate pathogenic gating pore current as an important contributor to ASD.

Results

Gating Charge Mutations in ASD. Five ASD probands with missense mutations in Arg gating charges in K_V7.3 were previously described (R227Q, R230C, and R236C) (4), and we identified four additional missense mutations in gating charges of K_V7.3 in the Simons Foundation genome database gnomAD (34) (R230H, R236C, and R236L; *SI Appendix*, Fig. S1). To search for additional gating charge mutations, we aligned the S4 segments of voltage-gated ion channels with mutations identified in neurodevelopmental disorders (https://denovo-db.gs.washington.edu/denovo-db) in channels with an autism gene score greater than 3 (gnomAD) (34). Surprisingly, 16 voltage-gated ion channels with autism gene scores of 3 or higher were identified as having gating charge mutations with a cumulative allelic frequency in genomAD of 1.46×10^{-3} (*SI Appendix*, Fig. S1). The high frequency of these mutations in Arg gating charges from a wide array of voltage-gated ion channels suggests that they may have a common pathogenic mechanism, similar to gating pore current in periodic paralysis.

Gating Pore Currents in a Bacterial K_V7 Channel. Gating pore currents are very small, typically in the range of 1% of the central pore current (21). We previously studied pathogenic gating pore currents in skeletal muscle Na_V1.4 channels by inserting the disease mutations into a bacterial sodium channel, which resulted in robust gating pore currents that could be easily measured in whole-cell voltage clamp (35, 36). Therefore, we searched for a bacterial K_V7 ortholog that could be expressed at high density in heterologous cells. Using a protein-based BLAST (Basic Local Alignment Search Tool) search, we found 254 closely related bacterial K_V7 channels, whose S4 segments have highly conserved gating charges, including the atypical Q in the third gating charge position (Fig. 1*A* and *Materials and Methods*). The K_V7 channel from *Oscillatoriales cyanobacterium* (K_V7Oc) is 29% identical and 49% similar in amino acid sequence to mammalian K_V7.3 over 281 amino acid residues, including the voltage sensor with Q in the position of R3, the pore, and all six transmembrane segments (*SI Appendix*, Fig. S2), but it lacks the large C-terminal regulatory domain characteristic of mammalian K_V7 channels. K_V7Oc was expressed in *Trichoplusia ni* insect cells (High Five cells) (37) and analyzed by whole-cell voltage clamp. The expressed channels conducted large outward potassium currents with characteristics similar to human K_V7 (hK_V7) channels (Fig. 1*B*; see *SI Appendix*, Fig. S7 for comparison). To assess the possibility that K_V7Oc/WT with the atypical Q in the position of R3 conducts gating pore current, we bathed Hi5 cells expressing K_V7Oc in an external solution containing 140 mM NaCl and an internal solution containing CsF, and we measured leak currents at a range of membrane potentials (Fig. 1*C*). Indeed, we observed a large outward gating pore current conducted by K_V7Oc/WT, beginning at −30 mV and increasing steadily into the positive voltage range (Fig. 1*C*). Remarkably, this gating pore current was completely blocked by mutating Q3 in the S4 segment to R3 (Fig. 1*D*), the more conventional amino acid at this position in other voltage-gated channels. These results demonstrate that Q3 is essential for gating pore conductance through the voltage sensor of wild-type K_V7 channels (Fig. 1*D*).

We introduced three mutations into K_V7Oc at the orthologous gating charge positions of hK_V7.3 ASD mutants (R1C, R2C, and K4C; Fig. 1*B* and *SI Appendix*, Fig. S1). All three mutations showed typical outward K^+ current with voltage dependence similar to WT (*SI Appendix*, Fig. S3). K_V7Oc/R1C

conducted wild-type outward gating pore current in the positive voltage range, similar to K_V7Oc/WT (Fig. 2*A*). Strikingly, this mutant also conducted a new inward gating pore current through the resting state of the voltage sensor in the negative membrane potential range (Fig. 2*A*).

Gating pore current is clearly distinguished from central pore current by the protocols used for recording leak currents. However, to further ensure that our measurements of gating pore current were not contaminated by the much larger central pore current, we blocked the central pore by inserting the mutation W196F in the ion selectivity filter, based on the *Shaker* K_V channel W434F mutation that locks the pore in an inactivated state (38) (*SI Appendix*, Fig. S4).

With Na^+ in the internal recording solution and impermeant *N*-methyl-D-glucamine (NMDG) in the extracellular solution, we recorded a robust outward gating pore current conducted by K_V7Oc/R2C/W196F in the positive membrane potential range (Fig. 2*B*). With external Na^+ and internal NMDG, recordings of K_V7Oc/R2C/W196F revealed a large inward gating pore current in the physiologically relevant negative membrane potential range from −10 to −100 mV (Fig. 2*C*). The amplitude of the pathogenic inward gating pore current was ∼4% of the central pore current, as estimated by dividing the gating pore current amplitude at −100 mV by the central pore current amplitude at +100 mV from the same cell, I_{gp}/I_K. This level of gating pore current is equivalent to 1% per mutant gating pore in tetrameric K_V7, as observed for the single-mutant gating pore in Na_V1.4 channels (21). As expected from the position of R2C in the S4 segment, inward gating pore current in the negative voltage range was observed at more positive stimulus potentials than for R1C, as required to drive R2 into the hydrophobic constriction site in the voltage sensor. Thus, both the R1C and R2C mutations in K_V7Oc cause a new gating pore current through the resting state of the voltage sensor in the negative membrane potential range.

Based on previous studies (22), we expected that K_V7Oc/K4C would conduct outward gating pore current at positive membrane potentials, as its modified gating charge moves outward into the hydrophobic constriction site in the activated state of the voltage sensor. Indeed, we observed a robust outward gating pore current for this mutant, with similar outward Na^+ current density to R2C (Fig. 2 *B* and *D*, gold). As

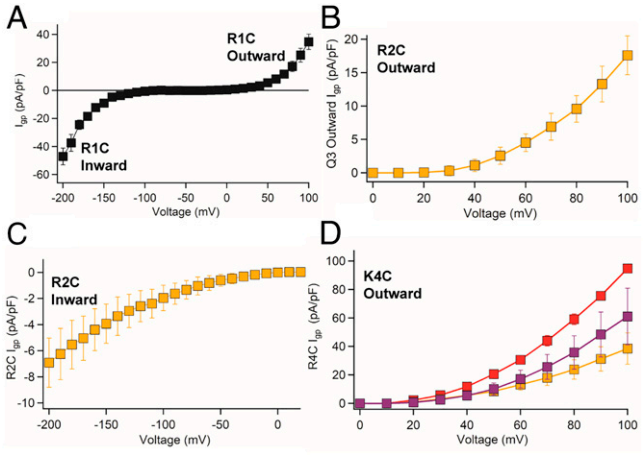

Fig. 2. Gating pore currents of ASD mutants in K_V7Oc. (*A*) Current-voltage (I-V) curve of K_V7Oc/R1C showing inward gating pore current starting from −50 mV carried by Na^+ and outward wild-type gating pore current, starting from +50 mV, carried by Cs^+. (*B* and *C*) I-V curves of outward and inward gating pore current of K_V7Oc/R2C carried by Na^+. (*D*) Ion selectivity of the outward gating pore current from K_V7Oc/R4C: Na^+ (gold), K^+ (purple), and Cs^+ (red). n = 7 to 10 cells.

previously observed for Na_V channel gating pore currents (36), we found that K_V7Oc gating pore currents are not highly selective. The ion selectivity sequence for K_V7Oc/K4C was $Cs^+ > K^+ > Na^+$ (Fig. 2*D*: K^+, purple; Cs^+, red; Na^+, gold). In contrast, the ion selectivity sequences were $K^+ > Cs^+ \sim Na^+$ for K_V7Oc/R2C compared to $Cs^+ \sim K^+ > Na^+$ for K_V7Oc/R1C and the wild-type gating pore of K_V7Oc/WT (*SI Appendix*, Fig. S5). Although gating pores are relatively nonselective among different monovalent cations, their pathogenic effects are caused by persistent leak of Na^+ into cells, leading to reduced sodium gradient, depolarization, and resulting alterations in action potential generation (21).

Double Gaps Cause Large Gating Pore Currents in Mutant K_V7 Channels. Why do mutant K_V7 channels associated with ASD conduct such large gating pore currents? The neighbors of gating charge mutations in the S4 segment greatly influence the size of the gating pore current they induce. For example, creating double gaps by mutating two sequential gating charge Arg residues in the S4 segment of K_V1 channels or Na_V1.2 channels to shorter hydrophilic amino acids leads to large gating pore currents (20, 39). The unusual amino acid sequence in gating charge positions 0 to 5 in the S4 segment of K_V7.3 (QRRQKR, Fig. 1*A*) allows single substitutions of R1Q, R2C, and K4C to create the double gaps QQ, CQ, and QC, respectively, and these double gaps generate larger gating pore currents than single gaps (*SI Appendix*, Fig. S6). Thus, the K_V7 channel is uniquely susceptible to mutations that cause large gating pore currents that are likely to be pathogenic because of the native Gln residues in gating charge positions that are typically occupied by large positively charged residues in other K_V channels.

Mutations in Human K_V7.3 Channels Induce Gating Pore Current. To test the hypothesis that gating pore currents are enhanced by ASD-associated mutations in human K_V7.3 channels, we generated mutations at the orthologous R1, R2, and R4 positions. We disabled the canonical pore using the I312R mutation (40), which completely blocked K^+ currents through the central pore in hK_V7.3 (*SI Appendix*, Fig. S7), and we used K^+ as the permeant ion to increase the size of the gating pore currents and compensate for the lower current amplitudes of hK_V7.3. The central pore currents for the hK_V7.3 ASD mutants were similar to the WT channels (*SI Appendix*, Fig. S8). The ASD-linked mutation hK_V7.3/R1Q (R227Q) conducted a substantial inward gating pore current in the resting state, starting from −40 mV and increasing with more negative potentials (Fig. 3*A*, red), as well as a substantial outward gating pore current in the positive voltage range (Fig. 3*B*, red). Like R1Q, the mutant K_V7.3/R1C also conducted a large inward gating pore current at negative membrane potentials (Fig. 4*B*). The hK_V7.3/R2C mutant (R230C) conducted inward gating pore currents, which were larger than R1Q at comparable membrane potentials (Fig. 3*A*, blue). Outward gating pore currents conducted by hK_V7.3/R2C were observed at potentials more positive than −100 mV and were larger than those for hK_V7.3/R1C (Fig. 3*B*, blue). These experiments show that both ASD-associated mutants, hK_V7.3/R1Q and hK_V7.3/R2C, conduct large, potentially pathogenic, inward gating pore currents in the physiologically significant −10- to −100-mV membrane potential range.

In contrast to the inward gating pore current created by the R1Q, R1C, and R2C mutations, the hK_V7.3/R4C mutation (R236C) conducted outward gating pore current that was first detected at −50 mV and increased at positive membrane potentials up to +100 mV (Fig. 3*C*). The outward gating pore current of hK_V7.3/R4C is not as large as that of K_V7.3/R2C measured under comparable conditions (Fig. 3*D*). The voltage onset of the hK_V7.3/R4C outward gating pore current at −50 mV corresponds to the threshold for central pore opening, where it

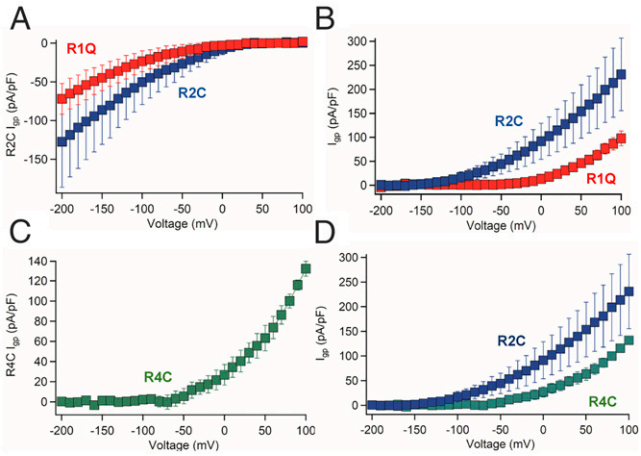

Fig. 3. Gating pore currents of ASD mutants in $hK_V7.3$. (*A*) I-V curves of $hK_V7.3$/R1Q and $hK_V7.3$/R2C inward gating pore current carried by K^+. Voltage onset for $hK_V7.3$/R1Q is −50 mV, while $hK_V7.3$/R2C inward gating pore current starts from 0 mV. n = 10 cells. (*B*) I-V curves of outward gating pore current of $hK_V7.3$/R1Q and $hK_V7.3$/R2C carried by K^+. n = 10 cells. (*C*) I-V curves of outward current of $hK_V7.3$/R4C carried by K^+. $hK_V7.3$/R4C outward current is carried by leak through the R4C and Q3 positions. n = 9 cells. (*D*) Comparison of I-V curves of outward gating pore current of $hK_V7.3$/R2C and $hK_V7.3$/R4C. $hK_V7.3$/R2C outward current is carried by leak through both the R2C and Q3 positions, while the $hK_V7.3$/R4C outward gating pore current is carried by leak through the R4C and Q3 positions.

would have most impact on K_V7 function (*SI Appendix*, Figs. S7 and S8). In this membrane potential range, inward Na^+ gating pore current would oppose the effects of outward K^+ gating pore current and the wild-type outward central pore current through hK_V7 channels and thereby disrupt their function.

Because of the physiological importance of the ion selectivity of gating pore current in mutant hK_V7 channels, we measured the Na^+ and K^+ gating pore currents through all four $hK_V7.3$ mutants (Fig. 4). Like K_V7Oc, gating pore conductance of ASD-associated mutants in $hK_V7.3$ channels is selective for K^+ over Na^+ (Fig. 4). Nevertheless, the substantial gating pore conductance for Na^+ would disrupt resting membrane potential and action potential firing. Overall, these findings show that WT $hK_V7.3$ conducts outward gating pore current and that three distinct ASD-associated gating charge mutations induce

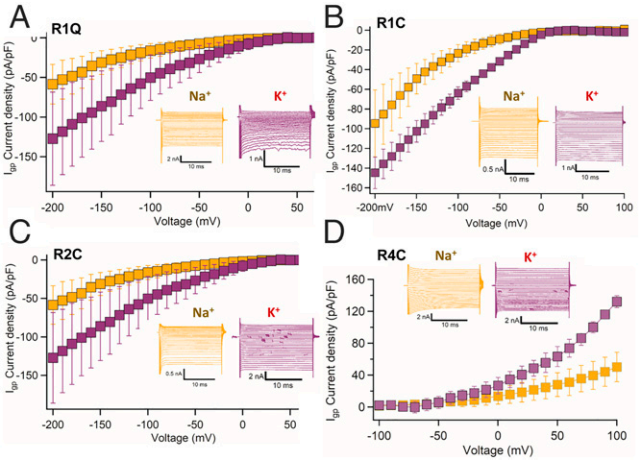

Fig. 4. Ion selectivity of gating pore currents of $hK_V7.3$ ASD mutants. (*A–D*) Ion selectivity for Na^+ and K^+ currents of $hK_V7.3$/R1Q, $hK_V7.3$/R1C, $hK_V7.3$/R2C, and $hK_V7.3$/K4C mutants. K^+ (purple) carries two- to threefold higher gating pore current density compared to Na^+ (yellow).

additional, potentially pathogenic, inward and outward gating pore currents with different voltage sensitivity and amplitude in the physiologically significant membrane potential range.

Altered Action Potential Firing Caused by $K_V7.3$ Mutants. VTA dopamine neuron activity is regulated by K_V7 channels (25, 41), and $K_V7.3$ subunit expression is associated with differences in social behavior in mice (42). Disruption of ASD-associated genes alters VTA dopamine neuron function (31, 32), further implicating these neurons in ASD etiology. Based on these observations, we asked whether expression of a human ASD-associated variant in $K_V7.3$ would alter the activity of these cells. Consistent with previous reports (26, 43), we found that ∼88% of dopamine neurons identified as tyrosine-hydroxylase–expressing cells also coexpress *Kcnq3* (*SI Appendix*, Fig. S9 *A* and *B*). To assess the impact of enhanced $K_V7.3$ gating pore currents on firing of action potentials in VTA dopamine neurons, we conditionally disrupted the endogenous $K_V7.3$-encoding gene in mice using a viral CRISPR/SaCas9 strategy (25) and conditionally reexpressed $hK_V7.3$/WT or mutant $hK_V7.3$/R2C via viral delivery (Fig. 5*A* and *SI Appendix*, Fig. S9 *C* and *D*). In these neurons, disruption of $K_V7.3$ subunits with CRISPR/SaCas9 (Fig. 5*A* and *Materials and Methods*) did not alter the proportion of spontaneously active cells, but substantially increased the frequency of spontaneous and evoked action potential firing (Fig. 5 *B–E*). Expression of $hK_V7.3$/WT rescued these effects. In striking contrast, $hK_V7.3$/R2C expression almost completely prevented spontaneous activity (Fig. 5 *B* and *E*), decreased firing in response to depolarizing current injection (Fig. 5 *D* and *E*), and increased the spike frequency accommodation during trains of action potential firing (Fig. 5 *D* and *F*). Notably, the opposing effects of disruption of $K_V7.3$ and introduction of $hK_V7.3$/R2C on excitability show that R2C-mediated decrements in dopamine neuron excitability cannot be attributed to a loss of function of $K_V7.3$. Through analysis of the characteristics of single evoked action potentials, we observed that mutation $hK_V7.3$/R2C prolonged action potential duration (Fig. 6 *A* and *B*) and reduced afterhyperpolarization (Fig. 6*D*) without affecting the peak spike amplitude (Fig. 6*C*). $hK_V7.3$/R2C also increased threshold (Fig. 6 *E* and *F*), reduced maximum rise velocity (Fig. 6*G*), and increased maximum decay velocity (Fig. 6*H*). Together, these decrements in action potential waveforms and firing patterns reflect severe disruption of the encoding properties of dopamine neurons expressing $hK_V7.3$/R2C.

How does inward gating pore conductance in $hK_V7.3$/R2C reduce action potential frequency? This extra leak conductance would serve as a shunt, increasing the threshold for action potential generation, blunting the afterhyperpolarization, and thereby reducing repriming of sodium channels during trains of stimuli (Figs. 5 *D–F* and 6 *A–H*), as shown previously for the effects of inward Na^+ current through the shunting gating pore conductance of the mutant skeletal muscle $Na_V1.4$ channel in hypokalemic periodic paralysis (21). Here, the R2C shunting conductance we have recorded is substantial at −50 mV (Figs. 3 *A* and *B* and 4*C*). The functional impact of this shunting conductance is seen best in the action potential phase plot for VTA dopamine neurons in Fig. 6*E*. Upon depolarization from −50 mV, the amplitude of the depolarization that drives action potential firing is depressed by the gating pore shunt conductance while the amplitude of the afterhyperpolarization that reprimes the sodium channels is also blunted by the gating pore conductance. This mechanism accounts precisely for the combination of increasing threshold in the depolarizing direction while at the same time decreasing the afterhyperpolarization in the hyperpolarizing direction. These effects would increase spike frequency accommodation, which extinguishes trains of action potentials prematurely and decreases action potential frequency and number. This pathogenic mechanism

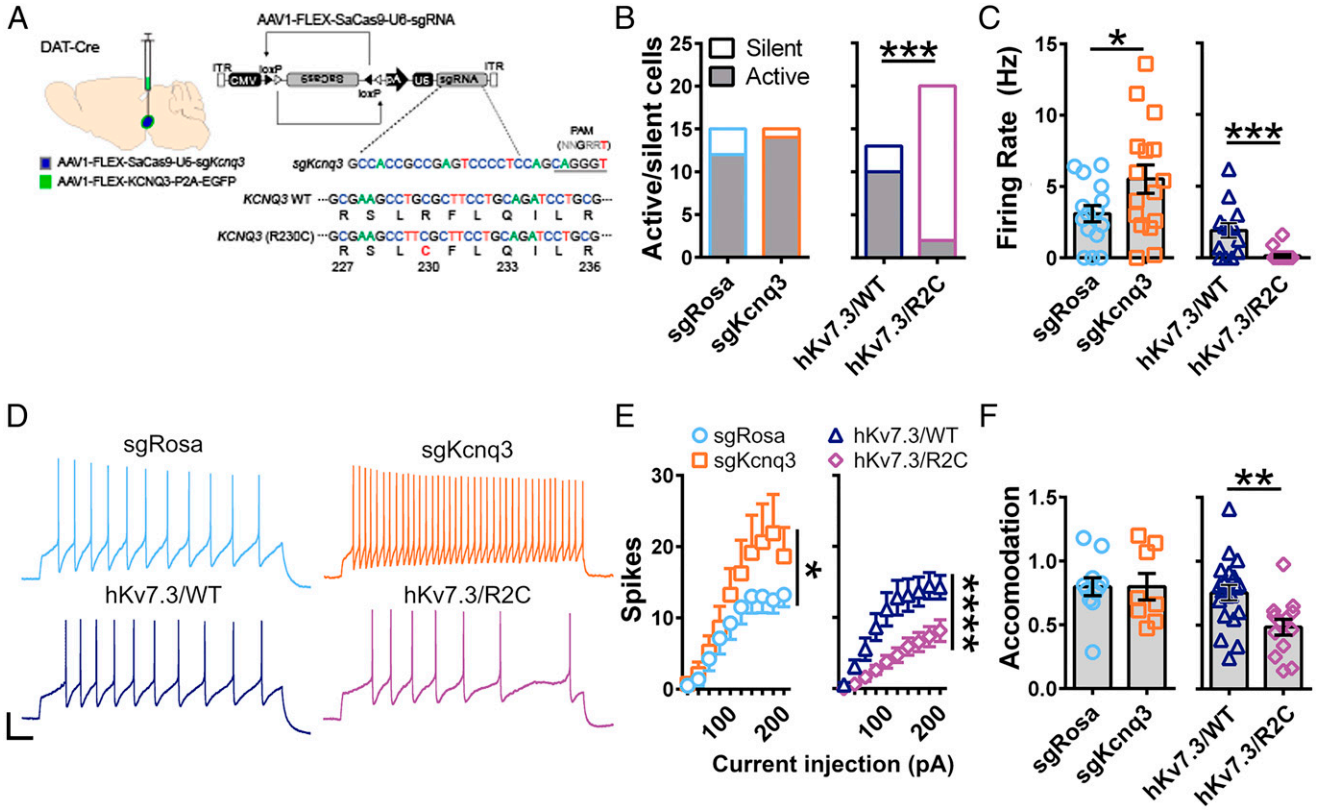

Fig. 5. Effects of $K_V7.3$/R2C ASD mutation on action potential generation in dopamine neurons in brain slices. (*A*) Schematic of $hK_V7.3$/WT and R2C reexpression strategy. (*B*) Number of cells that fired at least one action potential (active, gray) or no action potentials (silent, white) during a 10-s current clamp recording from dopamine neurons in which Rosa was inactivated (sgRosa), *Kcnq3* was inactivated (sgKcnq3), or *Kcnq3* was inactivated and either *KCNQ3*/WT ($hK_V7.3$/WT) or *KCNQ3*/R2C ($hK_V7.3$/R2C) was expressed. $P = 0.0002$; Fisher's exact test, two sided. (*C*) Firing rate of cells from *B*. sgRosa vs. sgKcnq3: $P = 0.0461$, Student's *t* test, two sided. $hK_V7.3$/WT vs. $hK_V7.3$/R2C: $P = 0.0002$, Student's *t* test, two sided. (*D*) Traces of firing in response to an injection of a 180-pA depolarizing current. (Scale bar: 20 mV, 100 ms.) (*E*) Number of action potentials fired during a 1-s depolarizing current injection from 20 to 200 pA in 20-pA increments. sgRosa vs. sgKcnq3: spikes × current injection interaction, $P = 0.049$, two-way repeated measures (RM) ANOVA. $hK_V7.3$/WT vs. $hK_V7.3$/R2C: spikes × current injection interaction, $P = 0.0001$, two-way RM ANOVA. (*F*) Accommodation index, calculated as the ratio of the interspike interval of the last two spikes in each train divided by that of the first two spikes. $P = 0.0052$, Student's *t* test, two sided.

would markedly alter input–output relationships of neurons and encoding of information in neural circuits.

Discussion

Pathophysiology of Mutations in K_V7 Channels. Previous studies show that impaired function of K_V7 channels causes hyperexcitability and epilepsy (10–13). In contrast to these previously described loss-of-function pathophysiological effects of K_V7 mutations, we have found $hK_V7.3$ gating pore mutations in patients with ASD that do not have epilepsy (4). Opposite to the increased excitability caused by loss of $K_V7.3$, the gain-of-function gating charge mutants described here cause an unexpected gating pore current and a profound decrease in neuronal excitability. This is a characterization of a K_V7 mutation that decreases neuronal excitability and therefore is unlikely to produce hyperexcitability and epilepsy. Moreover, based on the gene sequencing of trios that identified K_V7 gating charge mutations in individuals with ASD, and additional identification of these mutations in affected individuals in genomAD (2–4, 34), our study directly implicates gating pore currents conducted by these mutations in the pathogenesis of this disorder.

Functions of K_V7 Subunits in the VTA. The $K_V7.2$ and $K_V7.4$ channels subunits have been previously shown to be expressed in the VTA by immunohistochemistry (44, 45). Similar to $K_V7.2$/7.3, $K_V7.3$/7.4 heteromeric channels have higher conductance than K_V7 homomers (7, 46). Our previous analysis of cell-type selective messenger RNA levels in VTA dopamine neurons detected $K_V7.3$ as the most prominent K_V7 subunit expressed in these cells (47), consistent with the availability of $K_V7.3$ to form heteromers with either $K_V7.2$ or $K_V7.4$. Notably, both $K_V7.2$ and $K_V7.4$ have a Q at the third gating charge position; thus, we expect that these K_V7 channels also conduct wild-type outward gating pore current, as we have shown here for $K_V7.3$. Consistent with our results with CRISPR/Cas $K_V7.3$ loss of function, previous studies found that inhibition of K_V7 channels increases excitability of VTA neurons (45), similar to genetic inactivation of $K_V7.4$ (26). In contrast, activation of K_V7 channels decreases dopamine neuron activity in vivo (24), which is consistent with the effects we observed with the $hK_V7.3$/R2C gating pore current gain-of-function mutation. In addition to regulating action potential firing, K_V7 channels also regulate dopamine autoinhibition (48) and evoked dopamine release (49); thus, K_V7 gating charge mutations in ASD are likely to have multiple effects on dopamine neuron physiology.

Potential Effects of K_V7 Gating Pore Conductance at Axon Initial Segments. In addition to the disruption of action potential firing in dopamine neurons we have described here, we expect major alterations in action potential firing and input–output relationships in other types of neurons. K_V7 channels are clustered at axon initial segments where they control the resting membrane potential and action potential generation (50). In the well-studied

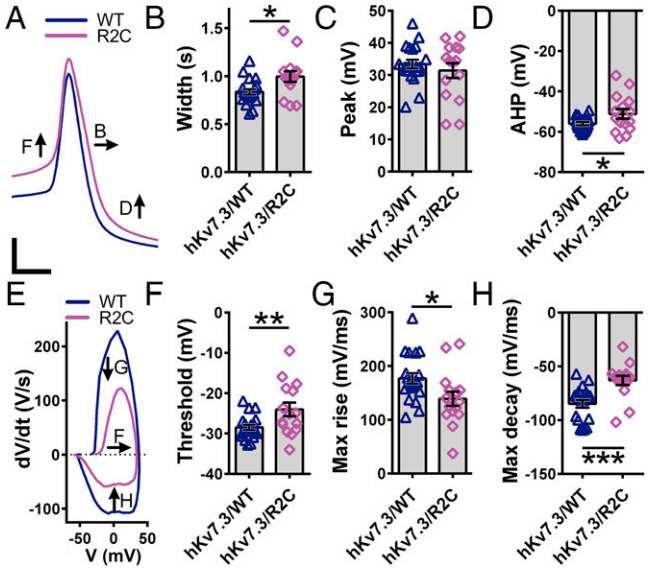

Fig. 6. Altered action potential shape in K_V7 mutants. (*A*) Traces of elicited action potentials recorded from dopamine neurons in which *Kcnq3* was inactivated and either *KCNQ3*/WT (WT) or *KCNQ3*/R2C (R2C) was expressed. (Scale bar: 20 mV, 1 s.) (*B*) Spike width at half-height. $P = 0.01$, Student's *t* test, two sided. (*C*) Peak spike amplitude. (*D*) Peak afterhyperpolarization. $P = 0.0371$, Student's *t* test, two sided. (*E*) Phase plots of elicited action potentials. (*F*) Threshold to fire an action potential. $P = 0.0099$, Student's *t* test, two sided. (*G*) maximum rise velocity. $P = 0.0248$, Student's *t* test, two sided. (*H*) Maximum decay velocity. $P = 0.0004$, Student's *t* test, two sided.

axon initial segment of neocortical pyramidal cells, K_V7 channels are concentrated at a density of 16.7 channels/μm^2 at the distal part of AIS and contribute 150 pS/μm^2 of membrane surface area when fully open, assuming a single channel conduction of 9 pS (50). The gating pore conductance we have measured is 0.4 pS per K_V7 channel; therefore, the density of 16.7 K_V7 channels/μm^2 would contribute 6.7 pS/μm^2 to the total resting membrane conductance at the axon initial segment. At the resting membrane potential, the K_V7 channels are ~4% open and they contribute ~6 pS/μm^2 to the resting membrane conductance (50). Thus, the conductance contributed by the gating pore current is slightly larger than the contribution of central pore conductance at the resting membrane potential. This level of gating pore conductance would have a major effect on the total resting membrane conductance and therefore would cause a substantial shunt for depolarizing and hyperpolarizing currents at the axon initial segment. The large effect on resting membrane conductance could easily cause increased threshold and decreased afterhyperpolarization in neocortical pyramidal neurons, as we have observed here for dopamine neurons.

K_V7 Gating Pore Currents in Autism. Based on our results, we expect that gating pore currents conducted by ASD-associated K_V7 mutants would strongly disrupt action potential firing in neurons in the hippocampus, neocortex, and elsewhere in which the clustering of mutant K_V7 channels at the axon initial segment would generate a large shunt conductance at this key site of action potential generation (50). These effects would alter the encoding properties of neurons and the excitation/inhibition balance in neural circuits. Alterations in excitation/inhibition balance in neural circuits are widely implicated in ASD (51–54). Therefore, disruption of the excitation/inhibition balance by gating pore currents in the axon initial segments of neurons may contribute to the broad range of behavioral and cognitive deficits in ASD. In addition to this potential impairment of neural circuit function generally, our results show directly that gating pore currents can disrupt action potential firing dramatically in spontaneously active neurons, like the dopamine neurons studied here, whose frequency of firing is strongly affected by small ionic currents near the resting membrane potential. Given the primary role of dopamine in regulation of social behavior, our findings suggest that the prominent social interaction deficits in individuals with these K_V7 mutations may be caused by specific deficits in mesostriatal function. Altogether, our results lead to the two-pronged hypothesis that gating pore currents in mutant K_V7 channels may impair social interactions directly by altering action potential firing in dopamine neurons and may have broader effects on cognitive function, repetitive behaviors, and communication skills in ASD by disrupting control of excitation/inhibition balance in a wide range of neural circuits.

Materials and Methods

Cloning and Expression. Bacterial K_V7Oc from *O. cyanobacterium* was identified in a protein BLAST search using the unique S4 sequence of K_V7 channels and further confirmed by sequence similarity to the pore domain of K_V channels and overall similarity to K_V7 channels. We chose the abbreviated name K_V7Oc in parallel with the names for bacterial Na_V channels, in which the first letters of the genus and species are appended to the channel designation (e.g., Na_VAb from *Arcobacter butzleri*). This K_V7 channel is listed under GenBank OIP70999.1: https://www.ncbi.nlm.nih.gov/protein/OIP70999.1?report=genbank&log$=prottop&blast_rank=1&RID=G5XKCWK5016. K_V7Oc was subcloned into the pFastBac vector (Invitrogen). Mutants were made in the K_V7Oc wild-type background. Human $K_V7.3$/WT and mutants were constructed in pFastBac vector, which provided expression at a high level. Single-point mutations were introduced using PCR (QuikChange; Agilent Technologies). All mutants were verified by sequencing the mutated cDNA.

Cellular Electrophysiology and Data Analysis. WT and mutant constructs were expressed in *T. ni* insect cells (High Five; Invitrogen), using recombinant baculovirus generated using the Bac-to-Bac system (Invitrogen). Cells were grown on 35-mm Petri dishes in Grace's insect medium (Gibco) supplemented with fetal bovine serum (FBS) (10%) and antibiotics (100 μg/mL streptomycin and 100 units/mL penicillin). Cells were infected by replacing the incubation medium with medium containing the virus encoding the WT or mutant channel (10 μg/mL). After 1 h, 2 mL of incubation medium was added to the virus-containing medium. Cells were maintained at 27 °C for at least 24 h before study. All constructs showed high expression, enabling us to measure gating current and gating pore currents 24 to 48 h after infection. Whole-cell sodium currents were recorded using an Axopatch 200 amplifier (Molecular Devices) with glass micropipettes (2 to 5 MΩ). Voltage clamp pulses were generated, and currents were recorded using Pulse software controlling an Instrutech ITC18 interface (HEKA). Data were analyzed using Igor Pro-6.35 (WaveMetrics). All experiments were performed at room temperature (20 to 24 °C).

For measurements of voltage-gated K^+ currents through the central pore of K_V7 channels, the holding potential was set to −100 mV, capacitance was subtracted using a P/-4 protocol, and series resistance was compensated 80 to 85% using internal amplifier circuitry. The intracellular pipette solution contained 140 mM KF, 10 mM Hepes, 10 mM EGTA, pH 7.4 (adjusted with CsOH). The extracellular solution contained 140 mM NMDG-F, 10 mM Hepes, 2 mM $CaCl_2$, pH 7.4 (adjusted with NaOH).

For gating pore current measurements, depolarized holding potentials for gating pore current measurements were maintained for 3 to 5 min before beginning measurements, and no series resistance compensation was used. The first experiments to detect the existence of wild-type gating pore current (Fig. 1) were performed using a physiological external solution containing 140 mM NaCl, 2 mM $CaCl_2$, 2 mM $MgCl_2$, 10 mM Hepes (pH 7.4) and an internal solution containing 35 mM NaCl, 105 mM CsF, 10 mM EGTA, 10 mM Hepes (pH 7.4). In subsequent experiments, the intracellular pipette solutions contained 140 mM KF, 10 mM Hepes, 10 mM EGTA, pH 7.4 (adjusted with CsOH), and the extracellular solution contained 140 mM NMDG-F, 10 mM Hepes, 2 mM $CaCl_2$, pH 7.4 (adjusted with NaOH). For ion substitution experiments, a concentration of 140 mM of the charge carrier (Na^+, K^+, or Cs^+) was present in either the recording pipette or the extracellular solution, and a 140-mM concentration of the same NMDG salt was present on the other side. Gating pore current was quantified for analysis at the end of each pulse. For R1C, R1Q, and R2C mutants, the linear leak current at positive potentials where I_{gp} was minimal was fitted with a straight line and subtracted from the total current to yield the nonlinear inward gating pore current. For R4C or R4K constructs, the

linear leak current at negative potentials was fitted using a linear regression equation and subtracted from the total leak current to yield the nonlinear outward gating pore current.

Virus Production. hKCNQ3 was cloned into a CMV-P2A-EGFP vector from pUC57-hKCNQ3 plasmid (GeneScript) using SalI and MfeI to produce pCMV-hKCNQ3-P2A-EGFP. Q5 site-directed mutagenesis (NEB Biolabs Inc.) was used to generate the following hKCNQ3 variants: I312R, R227Q/I312R, R227C/I312R, R230C/I312R, Q233R/I312R, and R236C/I312R. All mutagenesis primers were designed using the NEBaseChanger website (lowercase letter in forward primer indicates point mutation): R227Q forward, ACCTCCCTGCaAAGCCTGC-GC; R227Q reverse, GGCCAGAACATTGCCTTGGTTTC; R227C forward, CAC-CTCCCTGtgcAGCCTGCGCT; R227C reverse (LZ primer 1156), GCCAGAA-CATTGCCTTGGTTTCC; R230C forward, CGAAGCCTGtGCTTCCTGCA; R230C reverse, CAGGGAGGTGGCCAGAACATTG; Q233R forward, CGCTTCCTGCgGA-TCCTGCGC; Q233R reverse, CAGGCTTCGCAGGGAGGTG; R236C forward, GCA-GATCCTGtGCATGCTGCG; R236C reverse, AGGAAGCGCAGGCTTCGC; I312R forward, GTGGGGCCTGagaACACTGGCCA; I312R reverse, CACAGGGCATCTG-CATAG. The hKCNQ3-P2A-EGFP and hKCNQ3-R230C-P2A-EGFP were then cloned into a pAAV-CMV-FLEX plasmid using MfeI and BstBI with AAV2 inverted terminal repeat sequences (ITRs). For CRISPR viruses, AAV1-CMV-FLEX-SaCas9-U6-sgKcnq3 (Addgene Plasmid 159911) and AAV1-CMV-FLEX-SaCas9-U6-sgRosa26 (Addgene Plasmid 159914) were cloned as described (55, 56). All viruses were made using serotype AAV1 packaging vector as described (57).

Experimental Subjects. Male and female heterozygote DAT-cre mice (The Jackson Laboratory; B6.SJL-Slc6a3$^{tm1.1(cre)Bkmn}$/J, stock no. 006660) were used for this study. Mice were group housed on a 12-h light/dark cycle with ad libitum food and water. Experiments were carried out in accordance with the Institutional Animal Care and Use Committee at the University of Washington.

Surgery. During surgery, mice were under constant anesthesia (1.5 to 4%) and head fixed in a stereotaxic frame (Model 1900; David Kopf Instruments). Coordinates were standardized to bregma and anterior–posterior positions were adjusted using a correction factor (F = Bregma – Lambda/4.21). A Hamilton injection syringe was lowered 0.5 mm past the indicated depth and 0.5 μL virus was injected at a rate of 0.25 μL/min as the syringe was raised to the desired depth. VTA coordinates (relative to bregma) were $x = \pm 0.5$ mm, $y = -3.25$ mm, $z = -4.25$ mm. Mice were no less than 8 wk of age at the time of surgery.

Brain Slice Electrophysiology and Data Analysis. Slice electrophysiology experiments were carried out no sooner than 4 wk after surgery to allow for viral expression and gene inactivation. On the day of the experiment, mice were anesthetized with isoflurane and immediately decapitated. Brains were extracted and placed in ice-cold carboxygenated (95% O_2, 5% CO_2) artificial cerebral spinal fluid (aCSF) containing the following: 126 mM NaCl, 2.5 mM KCl, 1.2 mM $MgCl_2$, 2.4 mM $CaCl_2$, 1.4 mM NaH_2PO_4, 25 mM $NaHCO_3$, and 11 mM D-glucose. Kynurenic acid (1 mM) was added to the buffer for the slicing procedure. Horizontal midbrain slices (200 μm) containing the VTA were obtained using a vibrating microtome (Leica). Slices were incubated for at least 30 min at 34 to 36 °C with carboxygenated aCSF that also contained the NMDA receptor antagonist MK-801 (15 μM) unless noted otherwise.

Slices were placed in a recording chamber attached to an upright microscope (Olympus) and maintained at 34 to 36 °C with aCSF perfused at a rate of 2 mL/min. Dopamine neurons were identified by fluorescence (YFP or GFP) elicited by a MetaFluor software-controlled four-channel LED (Lumencor) with a fiberoptic that allows transmission of blue light through the microscope objective and yellow/green light to return through a filter cube to a Hamamatsu camera. The VTA was defined as the region 100 μM medial to the medial terminal nucleus of the accessory optic tract. Recording pipettes (1.5 to 4 MΩ resistance) were constructed from thick wall capillaries (World Precision Instruments) with a P-97 micropipette puller (Sutter). Whole-cell recordings were obtained using an intracellular solution containing the following: 130 mM K-gluconate, 10 mM Hepes, 5 mM NaCl, 1 mM EGTA, 5 mM Mg-ATP, 0.5 mM Na-GTP, pH 7.3, and 280 milliosmolar (mOsm).

Whole-cell recordings were acquired using an Axopatch 700B amplifier (Molecular Devices) at 10 kHz and filtered offline at 2 kHz. Membrane capacitance, series resistance, and input resistance were determined by applying a series of brief 5-mV depolarizing voltage steps. Liquid junction potential was corrected using the Multiclamp software automatic correction function. Spontaneous activity was recorded in current clamp mode (0 pA injection current) immediately after determination of membrane properties, and 10 s of activity was analyzed. To measure membrane excitability, a subset of cells was then held at −60 mV (to prevent spontaneous firing) and a series of depolarizing current injections (20 to 200 pA, 20-pA increments, 1 s duration) were delivered. Spike properties were calculated from the averaged spike waveform of the first three spikes elicited during the series of depolarizing current injections.

Data were analyzed using GraphPad Prism version 6. Two-way repeated measures ANOVA, Fisher's exact test, and Student's *t* tests were used, as described in legends for Figs. 5 and 6. For cell excitability data in Fig. 5 *D–F* the Prism ROUT outlier analysis was used to identify outlier cells that were removed from these graphs and analyses ($n = 3$ sgRosa, 1 sgKcnq3, 0 $hK_V7.3$/WT, 3 $hK_V7.3$). Data are represented as mean ± SEM.

Immunohistochemistry. Mice were anesthetized with Beuthanasia(Merck Sharp and Dohme Corp.) and perfused transcardially with ice-cold phosphate-buffered saline (PBS) followed by 4% paraformaldehyde (PFA). The brain was removed and placed in 4% PFA overnight and then transferred to 30% sucrose in PBS for 2 to 3 d. Brains were mounted in Tissue-Plus OCT Compound (Fisher) at −19 °C and frozen sections (30 μm) were cut using a cryostat (Leica). The following primary antibodies were used for protein detection: tyrosine hydroxylase (rabbit polyclonal, 1:2,000; Fisher Scientific) and GFP (chicken polyclonal, 1:10,000; Abcam). The slices were first blocked in 1× TBS with 0.3% Triton (TBST) and 3% normal donkey serum (TBST+NDS). Slices were incubated in primary antibody diluted in TBST+NDS overnight at 4 °C. The following day, brain sections were washed three times in TBST and then incubated with secondary antibodies (Jackson Immuno, Alexa Fluor-488; Cy3) diluted 1:250 in TBST+NDS and then washed three times and mounted onto slides using Fluoromount (Southern Biotech). Fluorescence was imaged using a Keyence BZ-X vision system.

In Situ Hybridization Using RNAscope. Wild-type C57BL/6 male and female mice (8 to 9 wk old) were used to map ion channel expression in the VTA using RNAscope (20). Brains were flash frozen in 2-methylbutane and stored at −80 °C. VTA sections were collected and processed for RNAscope (20 μm, coronal). Representative sections that spanned the VTA were selected for hybridization (anterior/posterior range: rostral, −3.1 mm; intermediate, −3.5 mm; caudal, −3.8 mm; according to the Paxinos atlas). Sections were prepared for hybridization per manufacturer's (Advanced Cell Diagnostics, Inc.) instructions using probes for Th (Mm-Th-C3) and Kcnq3 (Mm-Kcnq3-C1). Slides were coverslipped with Fluoromount with DAPI (Southern Biotech) and imaged using a Leica SP8X confocal fluorescence microscope. Analysis was performed in Cell Profiler 4.1.3 (https://github.com/CellProfiler/CellProfiler) using a modified image analysis pipeline for RNAscope (21).

Data Availability. All study data are included in this article and/or *SI Appendix*.

ACKNOWLEDGMENTS. This research was supported by research grants from the SFARI Program of the Simons Foundation (to L.S.Z. and W.A.C.) and the NIH (R35 NS111573 [to W.A.C.] and R01 MH104450 [to L.S.Z.]). Confocal imaging was performed on a Leica SP8X confocal fluorescence microscope at the University of Washington Keck Imaging Center, supported by NIH Grant S10 OD016240. We thank Dr. Eedann McCord (Pharmacology, University of Washington) for her initial bioinformatics analysis that identified bacterial K_V7 channels.

1. G. Schmunk, J. J. Gargus, Channelopathy pathogenesis in autism spectrum disorders. *Front. Genet.* **4**, 222 (2013).
2. B. J. O'Roak *et al.*, Sporadic autism exomes reveal a highly interconnected protein network of de novo mutations. *Nature* **485**, 246–250 (2012).
3. S. J. Sanders *et al.*, De novo mutations revealed by whole-exome sequencing are strongly associated with autism. *Nature* **485**, 237–241 (2012).
4. M. R. Geisheker *et al.*, Hotspots of missense mutation identify neurodevelopmental disorder genes and functional domains. *Nat. Neurosci.* **20**, 1043–1051 (2017).
5. T. J. Jentsch, Neuronal KCNQ potassium channels: Physiology and role in disease. *Nat. Rev. Neurosci.* **1**, 21–30 (2000).
6. P. Delmas, D. A. Brown, Pathways modulating neural KCNQ/M (K_V7) potassium channels. *Nat. Rev. Neurosci.* **6**, 850–862 (2005).
7. M. Bal, J. Zhang, O. Zaika, C. C. Hernandez, M. S. Shapiro, Homomeric and heteromeric assembly of KCNQ (K_V7) K^+channels assayed by total internal reflection fluorescence/fluorescence resonance energy transfer and patch clamp analysis. *J. Biol. Chem.* **283**, 30668–30676 (2008).
8. C. C. Hernandez, O. Zaika, G. P. Tolstykh, M. S. Shapiro, Regulation of neural KCNQ channels: Signalling pathways, structural motifs and functional implications. *J. Physiol.* **586**, 1811–1821 (2008).
9. H. C. Lai, L. Y. Jan, The distribution and targeting of neuronal voltage-gated ion channels. *Nat. Rev. Neurosci.* **7**, 548–562 (2006).

NEUROSCIENCE

10. H. Soh, R. Pant, J. J. LoTurco, A. V. Tzingounis, Conditional deletions of epilepsy-associated KCNQ2 and KCNQ3 channels from cerebral cortex cause differential effects on neuronal excitability. *J. Neurosci.* **34**, 5311–5321 (2014).
11. H. Soh *et al.*, Deletion of KCNQ2/3 potassium channels from PV+ interneurons leads to homeostatic potentiation of excitatory transmission. *eLife* **7**, e38617 (2018).
12. N. A. Singh *et al.*, A novel potassium channel gene, KCNQ2, is mutated in an inherited epilepsy of newborns. *Nat. Genet.* **18**, 25–29 (1998).
13. B. C. Schroeder, C. Kubisch, V. Stein, T. J. Jentsch, Moderate loss of function of cyclic-AMP-modulated KCNQ2/KCNQ3 K^+ channels causes epilepsy. *Nature* **396**, 687–690 (1998).
14. F. A. Vigil, C. M. Carver, M. S. Shapiro, Pharmacological manipulation of K_V7 channels as a new therapeutic tool for multiple brain disorders. *Front. Physiol.* **11**, 688 (2020).
15. L. Y. Jan, Y. N. Jan, Voltage-gated potassium channels and the diversity of electrical signalling. *J. Physiol.* **590**, 2591–2599 (2012).
16. V. Yarov-Yarovoy, D. Baker, W. A. Catterall, Voltage sensor conformations in the open and closed states in ROSETTA structural models of K^+ channels. *Proc. Natl. Acad. Sci. U.S.A.* **103**, 7292–7297 (2006).
17. U. Henrion *et al.*, Tracking a complete voltage-sensor cycle with metal-ion bridges. *Proc. Natl. Acad. Sci. U.S.A.* **109**, 8552–8557 (2012).
18. S. L. Venance *et al.*, CINCH investigators, The primary periodic paralyses: Diagnosis, pathogenesis and treatment. *Brain* **129**, 8–17 (2006).
19. F. Tombola, M. M. Pathak, E. Y. Isacoff, Voltage-sensing arginines in a potassium channel permeate and occlude cation-selective pores. *Neuron* **45**, 379–388 (2005).
20. S. Sokolov, T. Scheuer, W. A. Catterall, Ion permeation through a voltage-sensitive gating pore in brain sodium channels having voltage sensor mutations. *Neuron* **47**, 183–189 (2005).
21. S. Sokolov, T. Scheuer, W. A. Catterall, Gating pore current in an inherited ion channelopathy. *Nature* **446**, 76–78 (2007).
22. S. Sokolov, T. Scheuer, W. A. Catterall, Depolarization-activated gating pore current conducted by mutant sodium channels in potassium-sensitive normokalemic periodic paralysis. *Proc. Natl. Acad. Sci. U.S.A.* **105**, 19980–19985 (2008).
23. A. F. Struyk, S. C. Cannon, A Na^+ channel mutation linked to hypokalemic periodic paralysis exposes a proton-selective gating pore. *J. Gen. Physiol.* **130**, 11–20 (2007).
24. H. H. Hansen *et al.*, The KCNQ channel opener retigabine inhibits the activity of mesencephalic dopaminergic systems of the rat. *J. Pharmacol. Exp. Ther.* **318**, 1006–1019 (2006).
25. S. Koyama, S. B. Appel, Characterization of M-current in ventral tegmental area dopamine neurons. *J. Neurophysiol.* **96**, 535–543 (2006).
26. L. Li *et al.*, Selective targeting of M-type potassium K_v 7.4 channels demonstrates their key role in the regulation of dopaminergic neuronal excitability and depression-like behaviour. *Br. J. Pharmacol.* **174**, 4277–4294 (2017).
27. L. W. Hung *et al.*, Gating of social reward by oxytocin in the ventral tegmental area. *Science* **357**, 1406–1411 (2017).
28. L. A. Gunaydin, K. Deisseroth, Dopaminergic dynamics contributing to social behavior. *Cold Spring Harb. Symp. Quant. Biol.* **79**, 221–227 (2014).
29. J. A. McHenry *et al.*, Hormonal gain control of a medial preoptic area social reward circuit. *Nat. Neurosci.* **20**, 449–458 (2017).
30. K. Supekar *et al.*, Deficits in mesolimbic reward pathway underlie social interaction impairments in children with autism. *Brain* **141**, 2795–2805 (2018).
31. S. Bariselli *et al.*, Role of VTA dopamine neurons and neuroligin 3 in sociability traits related to nonfamiliar conspecific interaction. *Nat. Commun.* **9**, 1–15 (2018).
32. S. Bariselli *et al.*, SHANK3 controls maturation of social reward circuits in the VTA. *Nat. Neurosci.* **19**, 926–934 (2016).
33. D. Pavăl, I. V. Micluia, The dopamine hypothesis of autism spectrum disorder revisited: Current status and future prospects. *Dev. Neurosci.* **43**, 73–83 (2021).
34. K. J. Karczewski *et al.*, Genome Aggregation Database Consortium, The mutational constraint spectrum quantified from variation in 141,456 humans. *Nature* **581**, 434–443 (2020).
35. T. M. Gamal El-Din, T. Scheuer, W. A. Catterall, Tracking S4 movement by gating pore currents in the bacterial sodium channel NaChBac. *J. Gen. Physiol.* **144**, 147–157 (2014).
36. D. Jiang *et al.*, Structural basis for gating pore current in periodic paralysis. *Nature* **557**, 590–594 (2018).
37. T. M. Gamal El-Din, M. J. Lenaeus, K. Ramanadane, N. Zheng, W. A. Catterall, Molecular dissection of multiphase inactivation of the bacterial sodium channel Na_VAb. *J. Gen. Physiol.* **151**, 174–185 (2019).
38. E. Perozo, R. MacKinnon, F. Bezanilla, E. Stefani, Gating currents from a nonconducting mutant reveal open-closed conformations in Shaker K^+ channels. *Neuron* **11**, 353–358 (1993).
39. T. M. Gamal El-Din, H. Heldstab, C. Lehmann, N. G. Greeff, Double gaps along Shaker S4 demonstrate omega currents at three different closed states. *Channels (Austin)* **4**, 93–100 (2010).
40. F. S. Choveau, C. C. Hernandez, S. M. Bierbower, M. S. Shapiro, Pore determinants of KCNQ3 K+ current expression. *Biophys. J.* **102**, 2489–2498 (2012).
41. M. E. Soden *et al.*, Disruption of dopamine neuron activity pattern regulation through selective expression of a human KCNN3 mutation. *Neuron* **80**, 997–1009 (2013).
42. A. K. Friedman *et al.*, KCNQ channel openers reverse depressive symptoms via an active resilience mechanism. *Nat. Commun.* **7**, 1–7 (2016).
43. H. R. Wang *et al.*, KCNQ channels in the mesolimbic reward circuit regulate nociception in chronic pain in mice. *Neurosci. Bull.* **37**, 597–610 (2021).
44. E. C. Cooper, E. Harrington, Y. N. Jan, L. Y. Jan, M channel KCNQ2 subunits are localized to key sites for control of neuronal network oscillations and synchronization in mouse brain. *J. Neurosci.* **21**, 9529–9540 (2001).
45. T. Kharkovets *et al.*, KCNQ4, a K^+ channel mutated in a form of dominant deafness, is expressed in the inner ear and the central auditory pathway. *Proc. Natl. Acad. Sci. U.S.A.* **97**, 4333–4338 (2000).
46. C. Kubisch *et al.*, KCNQ4, a novel potassium channel expressed in sensory outer hair cells, is mutated in dominant deafness. *Cell* **96**, 437–446 (1999).
47. A. S. Chung, S. M. Miller, Y. Sun, X. Xu, L. S. Zweifel, Sexual congruency in the connectome and translatome of VTA dopamine neurons. *Sci. Rep.* **7**, 1–11 (2017).
48. M. Su *et al.*, K_V7.4 channel contribute to projection-specific auto-inhibition of dopamine neurons in the ventral tegmental area. *Front. Cell. Neurosci.* **13**, 557 (2019).
49. M. M. Jensen, S. C. Lange, M. S. Thomsen, H. H. Hansen, J. D. Mikkelsen, The pharmacological effect of positive KCNQ (K_V7) modulators on dopamine release from striatal slices. *Basic Clin. Pharmacol. Toxicol.* **109**, 339–342 (2011).
50. A. Battefeld, B. T. Tran, J. Gavrilis, E. C. Cooper, M. H. Kole, Heteromeric K_V7.2/7.3 channels differentially regulate action potential initiation and conduction in neocortical myelinated axons. *J. Neurosci.* **34**, 3719–3732 (2014).
51. S. Han *et al.*, Autistic-like behaviour in *Scn1a*$^{+/-}$ mice and rescue by enhanced GABA-mediated neurotransmission. *Nature* **489**, 385–390 (2012).
52. M. W. Antoine, T. Langberg, P. Schnepel, D. E. Feldman, Increased excitation-inhibition ratio stabilizes synapse and circuit excitability in four autism mouse models. *Neuron* **101**, 648–661.e4 (2019).
53. C. L. Gatto, K. Broadie, Genetic controls balancing excitatory and inhibitory synaptogenesis in neurodevelopmental disorder models. *Front. Synaptic Neurosci.* **2**, 4 (2010).
54. L. M. Lombardi, S. A. Baker, H. Y. Zoghbi, MECP2 disorders: From the clinic to mice and back. *J. Clin. Invest.* **125**, 2914–2923 (2015).
55. A. C. Hunker *et al.*, Conditional single vector CRISPR/SaCas9 viruses for efficient mutagenesis in the adult mouse nervous system. *Cell Rep.* **30**, 4303–4316.e6 (2020).
56. T. L. Stincic *et al.*, CRISPR knockdown of Kcnq3 attenuates the M-current and increases excitability of NPY/AgRP neurons to alter energy balance. *Mol. Metab.* **49**, 101218 (2021).
57. B. B. Gore, M. E. Soden, L. S. Zweifel, Manipulating gene expression in projection-specific neuronal populations using combinatorial viral approaches. *Curr. Protoc. Neurosci.* **65**, 4–35 (2013).